Macromolecules

pubs.acs.org/Macromolecules Article

# Dynamic Cross-Linking of Catalytically Synthesized Poly(Aminonorbornenes)

Nirmalendu Kuanr,[‖] Tanja Tomkovic,[‖] Damon J. Gilmour, Mitchell R. Perry, Shou-Jen Hsiang, Evelyne van Ruymbeke, Savvas G. Hatzikiriakos,* and Laurel L. Schafer*

Cite This: *Macromolecules* 2020, 53, 2649−2661 Read Online

ACCESS | Metrics & More | Article Recommendations | Supporting Information

**ABSTRACT:** Amine-functionalized polymeric materials have a wide variety of applications; however, the preparation of these materials is often plagued by laborious, multistep synthetic routes. Herein, a modified and improved synthetic protocol utilizes the hydroaminoalkylation reaction to catalytically assemble amine-functionalized monomers on a gram scale with 100% atom economy. Combined with ring-opening metathesis polymerization (ROMP), amine-functionalized polymers with varying electronic properties have been synthesized. Extensive rheological characterizations show that modification of the electronic properties of the amine substituent influences the bulk material properties through modification of hydrogen bonding and $\pi$-stacking interactions to afford dynamic cross-linking within the polymeric material. Tertiary amine-containing polymers display distinct rheological properties that differ from those of polymers with pendant hydrogen-bond-donating secondary amines. The profound viscoelastic effects that result from the incorporation of tunable dynamic interactions are presented.

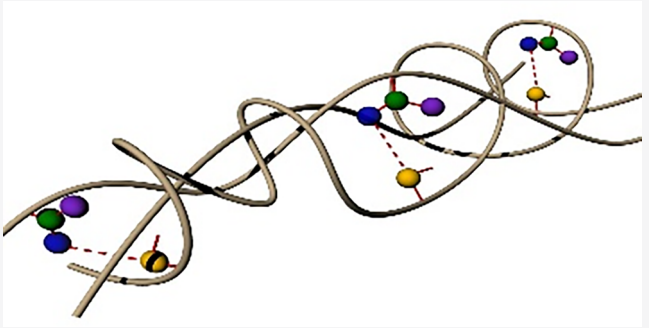

## INTRODUCTION

The chemical inertness, mechanical properties, and optimized syntheses of polyolefin materials have led to their widespread use. Ongoing research has sought to impart additional chemical functionality to increase the utility and scope of applications.[1,2] Specifically, the ability to controllably add polar functional groups to the nonpolar backbones of polyolefins is an intense area of investigation. Conventional approaches such as radical polymerization, anionic polymerization, and postpolymerization modification[3−6] have been widely investigated; however, these routes can show poor compatibility with the attempted incorporation of a polar functional group such as amines. Since the discovery of robust ruthenium-based olefin metathesis catalysts, ring-opening metathesis polymerization (ROMP) has emerged as a valuable tool for functionalized polymer synthesis.[7,8] However, due to established limitations in the use of amine substrates with Grubbs-type metathesis catalysts, this approach has only recently been disclosed for the synthesis of polymers containing unprotected amine functionality (Scheme 1).[9] Thus, while the substantial material advantages of amine incorporation are known, the controlled synthesis of amine-containing polyolefins has remained challenging. Furthermore, a predictive model for designing specific viscoelastic properties in this class of tunable materials is unknown.

The catalytic addition of amines to alkenes, hydroaminoalkylation, enables the selective formation of functionalized norbornene monomers in a single, atom-economic catalytic reaction while avoiding waste generation or the need for directing/protecting groups.[10−15] This approach offers advantages over alternative multistep protocols that rely on

**Scheme 1. Synthesis of Amine-Containing Monomers, Followed by ROMP**

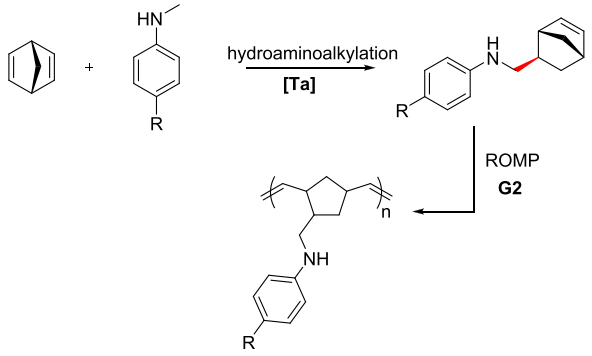


Received: October 11, 2019
Revised: February 17, 2020
Published: March 24, 2020







https://dx.doi.org/10.1021/acs.macromol.9b02158
*Macromolecules* 2020, 53, 2649−2661

stoichiometric transformations and the concomitant formation of byproducts.[9,10,13] Ready access to monomers suitable for ROMP offers an attractive 100% atom-economic route for the synthesis of amine-containing polymers (Scheme 1). However, easily assembled hydroaminoalkylation catalyst systems for high-yielding, multigram-scale syntheses of such monomers are unknown, and ROMP of unprotected amine-containing monomers has rarely been reported.[9,16,17]

Synthetic polymeric materials comprised of transient, weak, and reversible noncovalent interactions such as metal−ligand coordination,[18−20] inclusion complexation,[21−24] $\pi-\pi$ stacking,[25,26] and H-bonding[25,27] are used in a wide variety of applications. Extensive studies have been carried out to understand the usefulness of these noncovalent interactions for the assembly of supramolecular materials with a broad range of structures, properties, and applications. Stimuli-responsive properties such as pH-[28,29] and thermo-[30,31]responsiveness of such transiently cross-linked polymeric materials can be attributed to the reversibility of weak dynamic interactions within the material. Specifically, H-bonding in supramolecular polymers offers access to variable dynamic behavior as the strength of H-bonding can vary widely from highly dynamic to a quasicovalent nature.[32,33] Depending on the strength and reversibility of H-bonding, materials with reversible noncovalent interactions have found diverse applications as self-healing,[33−35] soft adhesive,[36] dynamic composite,[37] and self-assembly materials.[38−40]

Successful ROMP of the monomers generated by catalytic hydroaminoalkylation would result in new amine-functionalized polynorbornenes with H-bonding capabilities and tunable polymeric properties. Here, we report a high-yielding monomer synthesis using a mono-pyridonate tantalum amido catalyst that is generated in situ from commercially available starting materials.[13] Using ROMP, polynorbornenes bearing unprotected pendant secondary and tertiary amine groups can be obtained in high yields. These tunable polymeric systems can display enhanced solid-like viscoelastic behavior, as evidenced by melt rheology. The varied viscoelastic response among the resulting polymers indicates that the presence of the secondary amine is essential for the physical dynamic cross-linking of the polymers, providing key insight into H-bonding effects in bulk materials and transiently cross-linked polymer networks.[9] Strategies for how these materials can be strategically modified to target specific material properties are presented.

The application of associating polymers strongly depends on their mechanical and rheological properties, which are set between those of highly elastic, permanently cross-linked networks[41−43] and viscoelastic, temporarily entangled solutions.[44−47] These materials exhibit rich and diverse behavior that is based on the lifetime of associations, mobility of chains, polymer chain topology, and flow-induced properties.[48] The terminal relaxation of these polymer chains is governed by the average time needed for the hydrogen bond to dissociate, which is typically referred to as the lifetime of associations. The variable associating functionalized polymers presented in this work actively engage in H-bonding since a monomeric repeat unit consists of polar H-bond donor amine functionalities. Understanding of the chain dynamics of these systems is required to explain their complex dynamic behavior, which can be modeled using various theoretical approaches.[49,50] Using the comprehensive model developed by van Ruymbeke et al., the linear viscoelastic (LVE) behavior of secondary-amine-containing polynorbornenes can be understood by exploiting a small number of physical parameters.[51] The additional benefit from such modeling is the calculation of other molecular parameters useful in understanding the dynamics of associating polymers. Here, we show how this approach can be used to determine (i) the percentage of associating groups participating in the network formation and (ii) the various relaxation times such as lifetime of associations and the Rouse time governing the segmental dynamics of the chains.

## RESULTS AND DISCUSSION

**Monomer Synthesis.** To enhance the overall efficiency of accessing these dynamic materials, we first needed to improve hydroaminoalkylation catalysis. We had previously reported tantalum phosphoramidate precatalyst (**1**) as a preferred hydroaminoalkylation catalyst, as it could mediate this challenging C−C bond-forming reaction at room temperature (rt). However, **1** suffers from several challenges: (i) a tedious multistep synthesis and (ii) light- and heat-induced degradation, which results in a catalyst that suffers from low turnover numbers (TONs). These practical limitations prevented the synthesis of monomers on a multigram scale. Furthermore, selective mono-amination, while avoiding unwanted diamination of norbornadiene substrate, could only be achieved in moderate yields (ca. 50−60%). However, our group has shown that a 3-methyl pyridonate tantalum catalyst (**2**) can be used for efficient hydroaminoalkylation catalysis.[13] Catalyst **2** can be easily prepared by combining commercially available Ta(NMe$_2$)$_5$ and 3-methyl pyridone in situ, therefore avoiding the synthesis, isolation, purification, and storage of light- and heat-sensitive phosphoramidate catalyst **1**[13] (Scheme 2).

**Scheme 2. Comparison of Different Catalytic Systems Used for Monomer Synthesis**

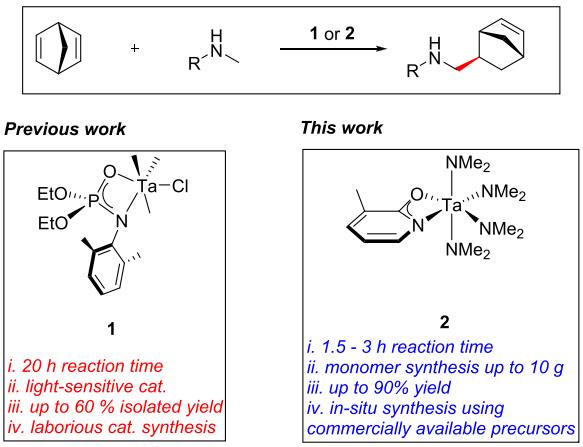


Under an inert atmosphere, the commercially available alkene and amine substrates can be added directly to a toluene solution of 10 mol % **2** (Scheme 3). The reaction mixture is heated at 130 °C for only 3 h to obtain products in a high yield (up to 90% after column chromatography). As the reactivity of the alkene is promoted by ring-strain, predominant selectivity is obtained through the higher strain present in the starting diene (34.7 kcal/mol) in contrast to the remaining alkene after mono-alkylation (27.2 kcal/mol).[52] To bias this selectivity further, excess equivalents of alkene are added. Excess amounts can be conveniently removed postreaction en vacuo. Using this


https://dx.doi.org/10.1021/acs.macromol.9b02158
Macromolecules 2020, 53, 2649−2661

**Scheme 3. Scope of Amine Substrates**[a]

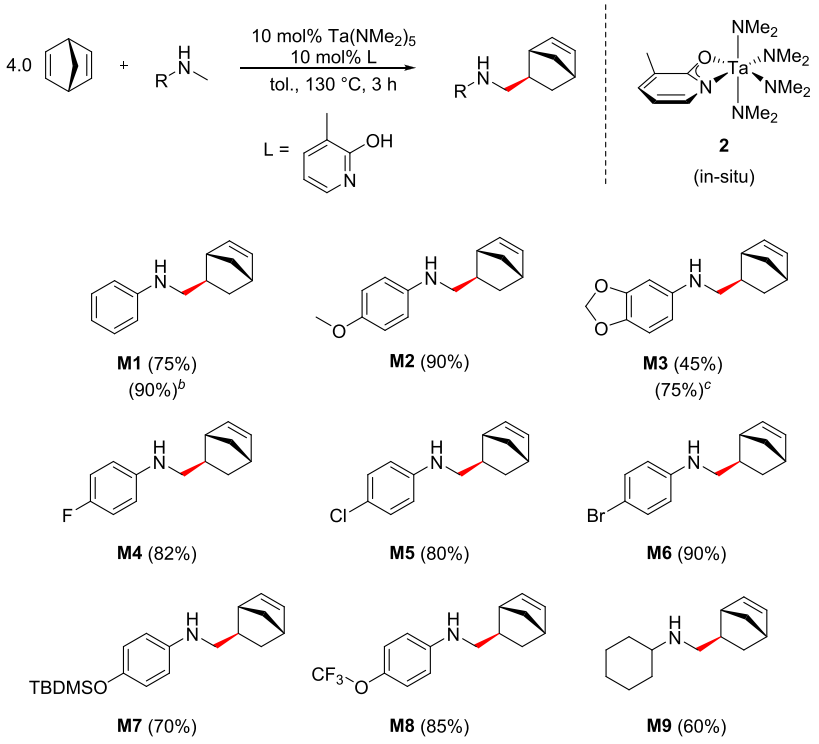


[a]Reaction performed in a 20 mL scintillation vial [b]1.5 h reaction time [c]4.5 h reaction time; yields represent isolated yields after flash column chromatography

**Scheme 4. Synthesis of Tertiary Amine-Containing Monomer M10**

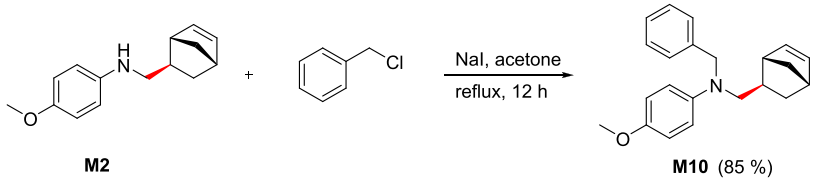


protocol, a series of electronically varied secondary amines were used for the amination of norbornadiene.

Catalyst **2** was used to functionalize norbornadiene with various para-substituted *N*-methylanilines. The parent *N*-methylaniline substrate was used to prepare **M1** in an excellent yield (90%) in only 1.5 h. Heating the **M1** reaction mixture for 3 h resulted in increased diaminated product. To demonstrate the robust performance of catalyst **2**, the reaction was performed using 55.5 mmol of *N*-methylaniline to afford multigram quantities of monomer **M1** with only a slightly diminished yield (7.75 g, 70% isolated yield). The reduction of yield in the scale-up reaction could be attributed to the size of the reaction vessel, reaction stirring rate, reaction headspace, etc. This monomer can be used to make a benchmark polymer (**P1**) that will be used for comparison purposes (vide infra). We have previously communicated that the effects of tuning amine electronic properties can result in variable H-bonding and viscoelastic properties in polymers,[9] and here, the scope of para substituents tested was expanded to gain further insight into these effects. The easily assembled catalyst **2** tolerates amines with electron-donating groups, such as **M2** and **M3**, as well as halide substituents in **M4**−**M6**. Monomer **M3** required 4.5 h of heating to obtain an improved yield of 75%. Highly polar and protic functional groups such as ketones and hydroxyl groups are known to be detrimental to the catalyst activity with early transition metal hydroaminoalkylation catalysts; however, the protected alcohol (−OTBDMS) amine variant (**M7**) was well tolerated (70% yield). The electronically varied trifluoromethoxy-substituted aniline derivative (**M8**) could also be isolated in an excellent yield. The more nucleophilic secondary *N*-methylcyclohexylamine proved somewhat more challenging for catalyst **2** and afforded **M9** in a 60% yield, with a significant amount of diaminated byproduct. To explore the importance of the role of the hydrogen-bond-donor ability of the various monomers, monomer **M2** was further alkylated to give a tertiary amine norbornene monomer **M10** (Scheme 4). Using Finkelstein conditions, benzyl chloride was used to alkylate **M2** in an 85% isolated yield. Using the highly robust, easy-to-assemble, and scalable catalyst **2**, various amine-containing norbornene monomers with a wide variety of electronic properties could be synthesized.

**Polymer Synthesis.** Polymerization by ROMP using **G2** was completed using **M1**−**M10**. Polymers were made with 100:1 monomer/initiator ratios ([M]/[I]) at room temperature (Table 1). For example, the complete consumption of monomer **M1** could be monitored by $^1$H NMR spectroscopy, where the disappearance of the olefinic resonances at 6.1 ppm of the monomer and the concomitant appearance of broad


https://dx.doi.org/10.1021/acs.macromol.9b02158
Macromolecules 2020, 53, 2649−2661

**Table 1. Various Substituted Aminonorbornene Polymers[e]**

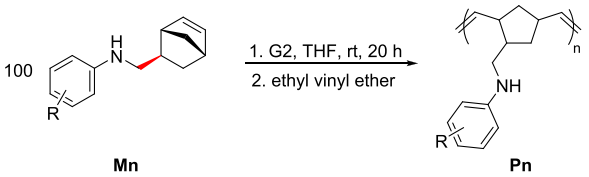


Mn Pn

| entry | monomer[a] | $M_n$[b] | DP[c] | $Đ$[d] |
|---|---|---|---|---|
| 1 | M1 | 90 300 | 453 | 1.30 |
| 2 | M2 | 81 700 | 357 | 1.14 |
| 3 | M3 | 82 000 | 337 | 1.25 |
| 4 | M4 | 28 800 | 132 | 1.10 |
| 5 | M5 | 36 400 | 155 | 1.15 |
| 6 | M6 | 99 300 | 357 | 1.16 |
| 7 | M7 | 107 900 | 327 | 1.27 |

[a]Monomer/initiator ratio 100:1. [b]Number-averaged molecular weight calculated from gel permeation chromatography (GPC). [c]Degree of polymerization (DP): $M_n$/MW g/mol. [d]Dispersity: $M_w/M_n$. [e]Values represent averages of triplicate experiments.

olefinic resonances at 5.3 ppm of **P1** indicate the completion of the reaction (see Figure S1, Supporting Information (SI)). After 24 h, the polymerization was quenched by the addition of excess ethyl vinyl ether and the **P1** was isolated by precipitation using a vortex of cold methanol. As we previously reported,[9] this constitutes a rare example of Ru-catalyzed ROMP with monomers bearing unprotected amine groups. In this case, the observed reactivity is obtained in part due to the diminished nucleophilicity of the aryl amine functionality.[53,54] This selective reactivity with aryl amines is supported by the fact that **M9**, an alkylamine, cannot be polymerized using **G2**.

Polymers **P1**−**P7** were all isolated as off-white/grayish flocculent solids that self-aggregate during precipitation. The resultant materials were evaluated by gel permeation chromatography (GPC) to determine the molecular weight. Unfortunately, trifluoromethoxyaniline-derivatized **P8** could not be precipitated, although, as determined by $^1$H NMR spectroscopy, complete polymerization of **M8** to **P8** had occurred (see Figure S30, SI). All of the polymers obtained were typically of higher molecular weights than the theoretical values predicted with a 100:1 [M]/[I] ratio (see Table S1). Good control over dispersity ($Đ$ = 1.1−1.3) was observed.

To explore the trend of the increased degree of polymerization (DP) than predicted, various polymers were prepared using varied [M]/[I] ratios with **M1**−**M3** (see Tables S1 and S2, SI). The DPs were consistently found to be multiple-fold higher than the theoretical values. The polymers (with [M]/[I] = 100; see Table S1) have DPs 3−5 times higher than the theoretical DP, although halide-substituted **P4** and **P5** are well-behaved systems, reflecting DPs close to the theoretical value, along with low levels of dispersity. We propose that the reduced nucleophilicity of the amine moiety, due to the strong electron-withdrawing effect of $F^-$ and $Cl^-$, may have less of an inhibitory effect on the ROMP catalyst. A reduction in electron-withdrawing features in **M6** and **M7** results in similar polymerization traits for **P6** and **P7**, as seen with **P1**−**P3**. Nevertheless, similar traits are seen for **P1**−**P3** polymers when prepared with lower [M]/[I] ratios of 50 and 25, i.e., DPs that are 2.5−5 times higher than theoretical DPs. Further, some small tailing of the major peak in the GPC chromatograms is consistent with increased dispersities, as seen in some cases (see Figures S34 and S35).

The molecular weight data suggest that there is inhibited catalyst initiation and/or the formation of dormant catalyst species resulting in a higher operative [M]/[I] ratio. We suggest that inhibition of some **G2** ROMP catalyst occurs in the presence of excess amine monomers. Grubbs et al. have reported slower rates of initiation relative to a rapid rate of propagation ($k_{ini} < k_p$) for **G2**.[55−58] Thus, inhibition and slow initiation could account for higher $M_n$ values for the polymers.

To probe the initiation of the catalyst, a stoichiometric reaction of **M2** and **G2** was monitored by $^1$H NMR spectroscopy (see Figure S3, SI). Indeed, the incomplete initiation of the catalyst was evidenced by the residual benzylidene proton resonance (19.3 ppm) of the uninitiated **G2** catalyst, which remains in spite of the formation of a slightly upfield alkylidene proton resonance (18.5 ppm) that is assigned to the alkylidene protons after metathesis. Based on their relative integration, it appears that as much as half of the ROMP catalyst sites remain uninitiated after even 20 h, suggesting that the polymerization proceeds efficiently with growth at the initiated sites, while some catalysts remain inactive. The incomplete initiation of catalyst ultimately results in the formation of polymeric material with a higher molecular weight than expected, with some variation in dispersity.

Next, the tertiary amine-containing monomer **M10** was subjected to our standard polymerization conditions (100 equiv of monomer, rt, tetrahydrofuran (THF)), followed by precipitation using cold methanol (Scheme 5). Polymerization

**Scheme 5. Polymerization of the Tertiary Amine-Containing Monomer**

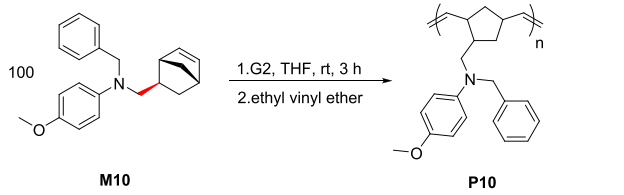


M10 P10

$M_n$ : 132,750 ($M_n$ theo. : 31,945)
$Đ$ : 1.16

of **M10** reached completion much faster than the secondary amine-containing monomers, with $^1$H NMR spectroscopy indicating complete consumption of **M10** in under 10 min (see Figure S2, SI). This observation suggests that sterically accessible secondary amine-containing monomers dramatically reduce the rate of ROMP as compared to the sterically hindered tertiary amine-containing monomers. The $M_n$ values obtained for **P10** from GPC were more than 4 times (the average of triplicate GPC runs was 132 750 ± 4000 g/mol) the molecular weight anticipated based upon the theoretically predicted molecular weight of 31 945 g/mol. Considering the narrow dispersity of 1.16, this class of sterically hindered tertiary amine-containing norbornene monomer is proposed to undergo very rapid propagation with hindered initiation. Qualitatively, the isolated polymer **P10** appeared very different from secondary-amine-containing polymers, as **P10** was obtained as grayish threads that did not aggregate.

With an optimized synthetic route for multigram polymer syntheses in place, we next pursued a complete and extensive rheological analysis of these materials to explore the effects of various H-bonding donors and acceptors in dynamic cross-linking of the polymeric materials.


https://dx.doi.org/10.1021/acs.macromol.9b02158
Macromolecules 2020, 53, 2649−2661

**Thermogravimetric Analysis (TGA) and Differential Scanning Calorimetry (DSC).** The thermogravimetry (TG) and derivative thermogravimetry (DTG) curves for all isolated polymer samples prepared using a monomer/initiator ratio of 100:1 are presented in the Supporting Information (see Figures S39–S41, SI). The results show a mass loss at temperatures above 250 °C and up to about 500 °C. Significant decomposition of polymer chains occurs at temperatures higher than approximately 300 up to 400 °C. However, the sharp mass loss of **P6** at 230 °C arises from the loss of the halide (−Br) group, which is not observed in the other halogen-substituted polymers (**P4** and **P5**). Finally, the sharp drop in the mass loss at temperatures above 400 °C is caused by the rapid degradation of the polymer backbone. The TG curves indicate that amine-containing polynorbornenes are thermally robust and do not decompose significantly until high temperatures of upward of 300 °C.

DSC thermograms (see Figures S40 and S41, SI) revealed the amorphous behavior of these secondary-amine-containing polynorbornenes, with glass transition temperatures, $T_g$, at about 70 °C (Table 2). Previous work on (*E*)- and (*Z*)-polynorbornenes indicated the values of $T_g$ to be about 40 °C.[59,60] The $T_g$ reported here is significantly higher due to the presence of associating H-bonding groups on every monomeric unit. However, $T_g$ for **P10**, with the tertiary amine incorporation, is around 45 °C, which is similar to that of unfunctionalized polynorbornene.[59]

**Table 2. Thermal Characteristics of Secondary and Tertiary Amine-Containing Polynorbornenes**

| entry | sample | DP[a] | $T_g$[b] (°C) | $T_{d,5\%}$[c] (°C) | $T_{d,50\%}$[d] (°C) |
|---|---|---|---|---|---|
| 1 | P1 | 470 | 60.7 | 351.3 | 429.1 |
| 2 | P2 | 387 | 60.6 | 350.8 | 419.2 |
| 3 | P3 | 330 | 82.8 | 305.0 | 456.7 |
| 4 | P4 | 131 | 71.8 | 361.6 | 431.7 |
| 5 | P5 | 151 | 74.8 | 290.1 | 416.1 |
| 6 | P6 | 373 | 83.3 | 234.8 | 361.9 |
| 7 | P7 | 326 | 76.4 | 355.6 | 421.1 |
| 8 | P10 | 495 | 46.9 | 309.5 | 408.8 |

[a]Degree of polymerization. [b]Glass transition temperatures estimated using DSC thermograms. [c]Thermal degradation at 5% mass loss. [d]Thermal degradation at 50% mass loss.

**Viscoelastic Properties.** Viscoelastic properties provide insight into intra- and intermolecular interactions in polymer dynamics. The rheological measurements were conducted on a stress-controlled Anton Paar MCR 702 device equipped with a cone partitioned-plate geometry and an air/nitrogen convection oven for accurate temperature control (±0.1 °C). All samples were oven-dried to ensure moisture elimination prior to the experiments. After drying, the samples were stored in a desiccator for a maximum of 24 h before performing the experiments. Dynamic time sweep tests were conducted to ensure the thermorheological stability (aging) of the samples. Over a period of 4 h, there was no change in the complex modulus, indicating no change in structure. The linear viscoelastic regions were determined using strain sweep experiments, which provide key information relating the polymer microstructure with chain dynamics (rheology). Dynamic moduli (storage, $G'$, and loss, $G''$) were obtained by applying various frequencies at a constant strain of 0.05 at various temperatures (from 100 to 200 °C). The time–temperature superposition principle was used to generate the master curves of these dynamic moduli (raw data can be found in Figures S49–S54) at the reference temperature of $T_g$ + 60 °C by applying both horizontal and vertical shift factors (Figure 1). First, to accurately determine the horizontal shift factors, $a_T$, the tan $\delta$ curves were shifted along the frequency axis for every temperature to superpose onto the reference curve ($T_g$ + 60 °C). Then, the complex modulus $|G^*|$ curves were shifted vertically to superpose to the reference curve to obtain the vertical shift factors, $b_T$. It is noted that the vertical shift factors applied were of the order of 1–1.6, and this is only for the two high temperatures of 180 and 200 °C (Tables S4–S8). This indicates that the plateau modulus exhibits a temperature dependence only at these high temperatures that most probably originates from the higher amounts of intermolecular associations. This suggests that at higher temperatures, while the hydrogen bonding strength decreases with an increase of temperature, the increased flexibility of the molecules creates more intermolecular associations at the expense of intramolecular ones. As further discussed below, the high number of functional groups is expected to form many intramolecular associations, posing entropic topological restrictions to molecules. Consequently, these restrictions lead to a few active functional groups available for intermolecular associations. The resulting master curves in Figure 1 reveal chain dynamics over a wide range of frequencies (time scales).

The horizontal shift factors for all samples, as determined in the generation of the master curves, are presented in Figure 2. They are found to be nearly identical for all associating polymers, indicating that they all belong to the same family of polymers and exhibit similar temperature dependency of their rheological properties. This allowed fitting of the data with the Williams–Landel–Ferry (WLF) equation, as is typically used for amorphous polymers, $\log a_T = -C_1(T - T_0)/(C_2 + T - T_0)$, using a single set of parameters, $C_1 = -13.01$, $C_2 = 246.4$, and $T_0 = 120$ °C, for the associating polymers, while different shift factors must be used for the reference **P10** sample, corresponding to $C_1 = 7.343$, $C_2 = 280.5$, and $T_0 = 110$ °C. This tertiary amine-containing polynorbornene (**P10**), which does not have an H-bond donor incorporated into each monomer, exhibits a similar $T_g$ to unfunctionalized polynorbornene, and classical behavior of slightly polydisperse polymer melts.[61] As such, **P10** is a useful reference polymer to probe the effect of H-bond donor functionality. Its terminal relaxation, which is the time for the relaxation of the whole polymer chain, was obtained at frequencies less than 1 rad/s. From modeling (presented below), its reptation time (nearly the longest relaxation time) was found to be around 1.6 s and the Rouse relaxation time of an entangled segment was found to be $2.5 \times 10^{-3}$ s. The molecular weight between entanglements was determined to be 28 000 g/mol, which corresponds to a plateau modulus equal to 100 kPa. Due to structural differences in the repeating units between various associating polymers and, therefore, differences in their flexibility, the molecular weight between entanglements is expected to vary for the associating polymers.

The presence of groups capable of forming reversible H-bonding associations delays relaxation significantly at time scales greater than $10^8$ s (Figure 1b–d and vide infra). As can be seen from Figure 1, the storage modulus $G'$ is independent of frequency over a wide range of frequencies. This plateau is a manifestation of the combined effects of entanglements and H-


https://dx.doi.org/10.1021/acs.macromol.9b02158
Macromolecules 2020, 53, 2649–2661

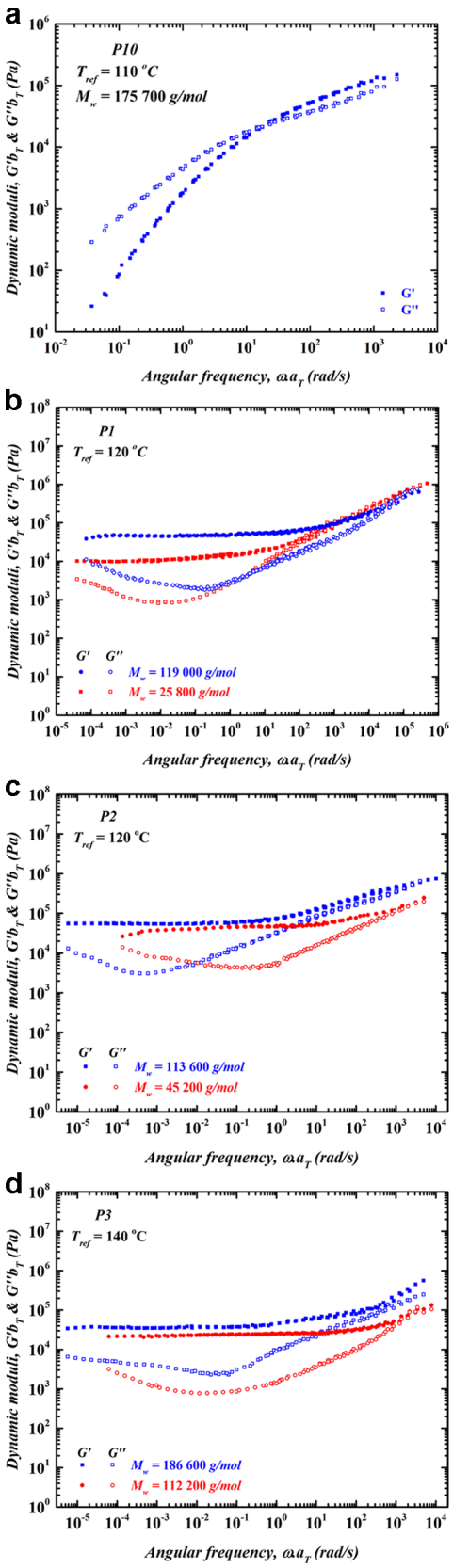


**Figure 1.** (a) Master curves of storage and loss moduli, $G'$ and $G''$, of tertiary amine-containing polynorbornene, **P10**, at the reference temperature of 110 °C. (b) Master curves of storage and loss moduli, $G'$ and $G''$, of samples **P1** with different molecular weights (red symbols: $M_w$ = 25 800 g/mol; blue symbols: $M_w$ = 119 000 g/mol) at the reference temperature of 120 °C. (c) Master curves of storage and loss moduli, $G'$ and $G''$, of samples **P2** with different molecular weights (red symbols: $M_w$ = 45 200 g/mol; blue symbols: $M_w$ = 113 600 g/mol) at the reference temperature of 120 °C. (d) Master curves of storage and loss moduli, $G'$ and $G''$, of samples **P3** with different molecular weights (red symbols: $M_w$ = 112 200 g/mol; blue symbols: $M_w$ = 186 600 g/mol) at the reference temperature of 140 °C.

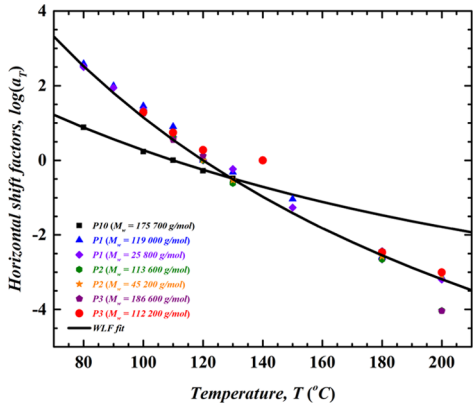


**Figure 2.** Temperature dependence of the horizontal shift factors used to construct the master curve for all samples with different molecular weights, $M_w$. The solid lines represent the WLF equation.

bonding associations, showing no tendency of relaxation at the experimentally accessible time scales. The number of functional groups capable of forming effective associations per chain, $Z_S$, could be, in principle, determined from the degree of polymerization (DP), where each monomer includes one H-bond donor. In such a case, we note that in polymers containing H-bond donors, $Z_S$ would be much larger than $Z_E$, the number of entanglements per chain. However, due to restrictions in the configurational entropy and formation of dangling chains and loops, not all pendant side groups effectively participate in the formation of H-bonding associations.[62] The segments between active associations, which have a molecular weight $M_S$, can, therefore, contain several monomers, as suggested by the low level observed for the plateau modulus. Since the linear viscoelasticity of these polymers is mainly governed by the associating groups, with $Z_S > Z_E$, the sample relaxation only occurs at the time larger than the association lifetime, $\tau_S$, which is observed to be larger than $10^6$ s.

Thus, although these polymers are slightly polydisperse, the plateau modulus (predominately due to reversible associations as discussed above) is obtained experimentally over a wide range of frequencies (several decades) due to the associations, the polymer segments of molecular weight $M_S$. Therefore, the effect of polydispersity on the chain dynamics is masked by the effect of the reversible associations. As explained by Zhang et al.,[63] associating entangled polymers with the molecular weight between associations smaller than the molecular weight between entanglements ($M_S < M_e$) exhibit two characteristic plateaus. The first plateau that we observe here is due to the presence of both associations and entanglements, where the end of the first plateau represents the lifetime associations. This plateau modulus is given by $G_N^0 (1 + Z_S/Z_E)$.[63−65] The second plateau is a manifestation of the entanglements, and it can be obtained at very low frequencies, which, in the present


https://dx.doi.org/10.1021/acs.macromol.9b02158
Macromolecules 2020, 53, 2649−2661

case, is inaccessible experimentally. For these samples, the role of entanglements is expected to be weak due to the high stiffness of the norbornene polymers. Furthermore, for the samples that are too short to be entangled ($M_w$ < 56 kg/mol), there is no second plateau at low frequency and the terminal flow regime is expected to take place directly after the first plateau.

The plateau modulus of associations and entanglements shows dependence on the molecular weight (Figure 1), i.e., increases with the increase of the molecular weight. As discussed later, this is mainly due to the larger fraction of dangling ends observed with low-molecular-weight samples, at constant $M_S$. Therefore, longer chains contain relatively more segments trapped between two intermolecular associations or entanglements, thus leading to a higher plateau consistently for all structures.[66] The functional groups along the chains also influence the Rouse relaxation of segments between stickers (associations) at the high-frequency regime, which also depends on the molecular weight. However, in all cases, the Rouse scaling $G' \approx G'' \sim \omega^{0.5}$ is clearly obtained.

As mentioned above, the plateau modulus strongly depends on the structure (repeating unit), as can be seen in Figure 3.

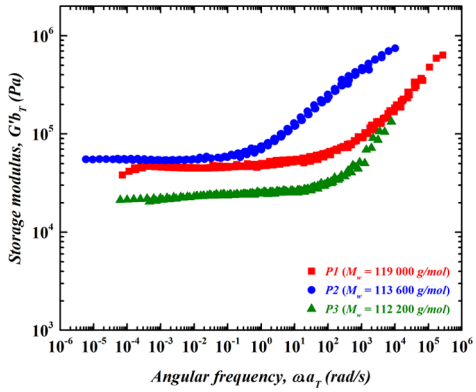


**Figure 3.** Master curves of storage modulus of samples **P1**−**P3** that have similar molecular weights (**P1**: red symbols, $M_w$ = 119 000 g/mol; **P2**: blue symbols, $M_w$ = 113 600 g/mol; and **P3:** green symbols, $M_w$ = 112 200 g/mol). The reference temperature is $T_g$ + 60 °C.

Three polymers **P1**−**P3** of similar molecular weights are compared. **P3** has less mobility, as determined by its higher $T_g$, and as would be predicted by its multiple sites for associations as well as a varied electronic structure that impacts H-bonding character. Although it potentially may create more and stronger associations, topological restrictions possibly due to more intramolecular associations cause the formation of fewer ones, which affects the magnitude of the plateau modulus. On the other hand, **P2** has both amine and methoxy groups capable of creating strong H-bonds, while retaining its higher flexibility. As a result, it possesses the highest modulus.

**Linear Viscoelastic Behavior Modeling.** To understand the complex chain dynamics of associating polymers, various theoretical models have been proposed. Cates et al. studied the dynamics of supramolecular networks by considering reversible scission and recombination of associating groups.[49,50,67] However, some experimental studies have shown the qualitative and quantitative limitations of this model.[68,69] Rubinstein, Colby, Leibler, and Semenov[50,66,70] further extended Rouse and reptation models, developing a comprehensive theory of reversible associations.[71,72] They derived scaling laws that relate the various relaxation times and viscosity to the number of reversible associations including entanglements and H-bonding interactions. These scaling laws can successfully describe the complex dynamics of currently studied systems that form strong transient supramolecular networks.

The linear viscoelastic (LVE) behavior of amine-functionalized polynorbornenes can be predicted using the time-marching algorithm (TMA). The TMA model is basically a tube model developed by Doi et al.[71] This algorithm has been developed by van Ruymbeke et al. for predicting the LVE behavior of entangled polymers with various architectures such as linear, star, tree-like, H, and pom−pom polymers[51,73,74] and can be extended to sticky polymer chains.[51] In such a case, in addition to the material parameters $M_e$, $G_N^0$, and $\tau_e$, the average molecular weight between associations, $M_S$, must be determined. As discussed above, for entropic reasons, it is almost impossible for each repeating unit to form reversible associations. Furthermore, it is expected that the chains contain a large fraction of intramolecular associations, leading to the formation of several small, unentangled loops. These internal loops probably also affect the average molar mass between two entanglements, which is expected to increase, compared to the reference sample, reducing, even more, the number of entanglements per chain. Therefore, in the model, it is assumed that entanglements play a negligible role in the dynamics of these polymers and both the influence of the effective stickers and the possible entanglements can be taken into account by a single-fit parameter $M_x$, which represents the average molar mass between a sticker or an entanglement, i.e., $M_x = (M_e^{-1} + M_S^{-1})^{-1}$, with $M_x \approx M_S$.

In the case of very long chains, the corresponding value of the plateau modulus is well approximated by $\rho RT/M_x$, with $\rho$ being the density. However, the samples studied here are too short to ignore the influence of dangling ends. Therefore, to determine the plateau level, the model[65] starts from the probability $p_{ass} \approx (M_x/m_0)^{-1}$ that a monomer creates an interchain association ($m_0$ is the molar mass of a monomer). Based on the MWD (assumed log mean), a large ensemble of chains is then created and associating units are placed randomly along their backbone. The molecular segments are then sorted into different categories, i.e., chains with no intermolecular associations, dangling ends, and chain segments trapped between two associated stickers, which are used as input data to determine the corresponding viscoelastic behavior, following ref 51. In practice, this model is used as an "inverse model", i.e., the best values of $M_x$ and $\tau_e$ are determined to minimize the discrepancy with the experimental data.

In view of the extension of the plateau at frequencies lower than $10^{-5}$ rad/s (time scales of several days), the lifetime of associations is taken as infinity in the model for practical reasons to minimize the number of free parameters. Consequently, the chain relaxation that starts to appear at a low frequency for some of the samples is not captured by this approach.

Only the data at low temperatures are modeled; essentially, the data at temperatures need no vertical shift to fall on the master curve ($T$ < 180 °C). The reason is that the TMA model does not allow for the temperature dependence of the plateau modulus. The values of the parameters calculated from the TMA algorithm at a reference temperature of 110 °C are listed in Table 3.


https://dx.doi.org/10.1021/acs.macromol.9b02158
Macromolecules 2020, 53, 2649−2661

**Table 3. Molecular Properties and Characteristic Relaxation Times of Various Polymers**

| entry | sample | $M_w$[a] (g/mol) | $_N^{G0}$[b] (kPa) | $M_x$[c] (g/mol) | $\tau_e$[d] (s) |
|---|---|---|---|---|---|
| 1 | **P1** | 25 800 | 14 | 12 500 | $5.0 \times 10^{-3}$ |
| 2 | | 119 000 | 53 | 20 000 | $1.8 \times 10^{-3}$ |
| 3 | **P2** | 45 200 | 55 | 12 500 | $10^{-2}$ |
| 4 | | 113 600 | 63 | 20 000 | $6.0 \times 10^{-1}$ |
| 5 | **P3** | 112 200 | 25 | 28 000 | $6.2 \times 10^{-2}$ |
| 6 | | 186 600 | 40 | 28 000 | $3.3 \times 10^{-3}$ |
| 7 | **P10** | 175 700 | 100 | | $2.5 \times 10^{-3}$ |

[a]Number-averaged molecular weight calculated from GPC. [b]Plateau modulus due to associations. [c]Molecular weight between associations and entanglements. [d]Rouse time of a segment with a molecular mass of 28 kg/mol.

The predictions of the TMA model are plotted and compared with the experimental data in Figure 4a–d. They are well matched with the data in cases of H-bond donor-containing polymers. It is worth noting that **P10**, with no H-bond donor, exhibits delayed terminal relaxation (Figure 4a), as indicated by not following the scaling $G' \propto \omega^2$, $G'' \propto \omega$ (characteristics of terminal relaxation). This deviation from the scaling can be attributed to $\pi-\pi$ stacking interactions.[75]

The results obtained for samples **P1** are shown in Figure 4b. To correctly describe the high-frequency Rouse relaxation, a slightly larger value of $\tau_e$ is used, $\tau_e = 5 \times 10^{-3}$ s, compared to the reference sample. It must be noted that in the present case, $\tau_e$ is not related to entanglements specifically, but rather represents the time that a molecular segment of the molar mass of $M_e$ = 28 kg/mol would need to relax by (sticky) Rouse. A good description of the viscoelastic curves is obtained by considering that the average molar mass between two intermolecular junctions is equal to 12 and 20 kg/mol for the **P1** sample with the low or the high molar mass, respectively. As already mentioned, these molar masses are rather high if we consider that each unit is carrying a sticker. As a general trend for all samples, it seems that the higher the molar mass of the chain, the higher the average molar mass between two effective stickers should be considered to obtain optimum data description. In the model, the relaxation of the dangling ends is taking place at the intermediate frequency. Thus, only the molecular segments trapped between two effective stickers contribute to the elastic plateau. This explains why the level of the plateau modulus of sample **P1** ($M_w$ = 25 800 g/mol) is lower compared to sample **P1** ($M_w$ = 119 000 g/mol), despite its larger probability to create intermolecular associations: due to the short length of the chains, the fraction of dangling ends is high.

Figure 4c presents the results obtained for the **P2** samples. Similarly, as for the **P1** samples, the average molar mass between two intermolecular associations is found to be equal to 12.5 and 20 kg/mol for the low and high molar mass samples, respectively. For these samples, the Rouse dynamics is observed to be slower than the relaxation of the reference sample and the **P1** samples, corresponding to $\tau_e = 10^{-2}$ s (for **P2** $M_w$ = 45 200 g/mol) and $6 \times 10^{-1}$ s (for **P2** $M_w$ = 113 600 g/mol). Figure 4d compares the theoretical and experimental data for the **P3** samples. Interestingly, good agreement is found by considering a rather large value of $M_x$ (of 28 kg/mol). This result suggests that the ratio between inter- and intra-associations is lower for this sample.

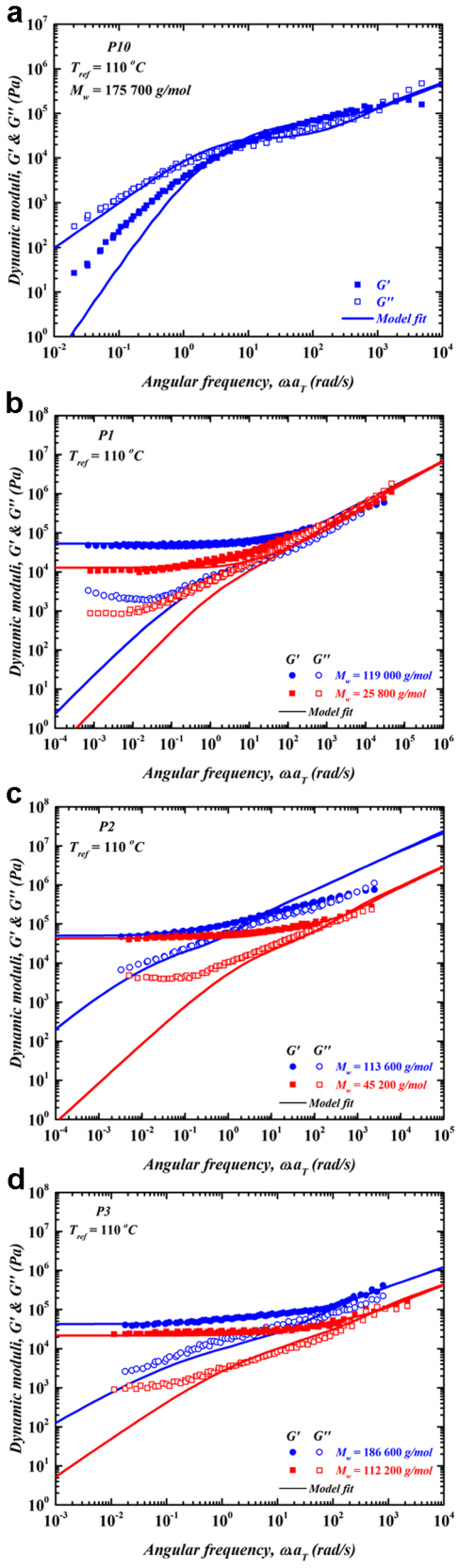


**Figure 4.** (a) Master curves of storage and loss moduli, as presented in Figure 1, along with the TMA model fit (solid lines), of tertiary amine-containing polynorbornene, **P10** ($M_w$ = 175 700 g/mol). (b) Master curves of storage and loss moduli, as presented in Figure 1, along with the TMA model fit (solid lines), of samples **P1** with different molecular weights (red symbols: $M_w$ = 25 800 g/mol; blue


https://dx.doi.org/10.1021/acs.macromol.9b02158
Macromolecules 2020, 53, 2649–2661

**Figure** 4. continued

symbols: $M_w$ = 119 000 g/mol). (c) Master curves of storage and loss moduli, as presented in Figure 1, along with the TMA model fit (solid lines), of samples **P2** with different molecular weights (red symbols: $M_w$ = 45 215 g/mol; blue symbols: $M_w$ = 113 677 g/mol). (d) Master curves of storage and loss moduli, as presented in Figure 1, along with the TMA model fit (solid lines), of samples **P3** with different molecular weights (red symbols: $M_w$ = 112 200 g/mol; blue symbols: $M_w$ = 186 600 g/mol).

**Extensional Rheology.** The results of the extensional rheology for all samples are depicted in Figure 5. The solid lines represent the linear viscoelastic envelope determined by fitting the dynamic moduli data (Figure 1) using the multimode Maxwell model (the best-fit parameters, $\lambda_i$ and $G_i$, are given in Table S3, Supporting Information). In comparison to tertiary amine-containing polynorbornene, **P10**, samples **P1**−**P3** contain polar groups capable of forming extensive H-bonding associations. **P10**, a reference sample that does not contain an H-bond donor, shows no strain hardening in comparison to **P1**−**P3**. The terminal zone for the **P10** sample (Figure 1a) was not completely achieved, which might be due to the presence of very weak electrostatic interactions between polarized aromatic rings in $\pi-\pi$ interactions.[75] Although the terminal relaxation was not achieved for **P10**, the corresponding LVE envelope shows flattening, essentially asymptotically approaching zero shear viscosity. As noted above, the tensile stress growth coefficient at different Hencky strain rates follows the LVE envelope, which is the typical behavior of linear polymers (no strain-hardening effects), although, at higher Hencky strain rates (unable to reach), strain hardening could have been obtained.[61] Typically, the Weissenberg number, $W_i$, defined as the Hencky strain rate, $\dot{\varepsilon}$, times the terminal relaxation time, $\tau_{rep}$, is used as a criterion for strain hardening, that is, for $W_i$ > 0.5, strain hardening is expected.[48]

In contrast to **P10**, samples **P1**−**P3** (Figure 5b−d) exhibit strong strain hardening with tensile stress growth coefficients, $\eta_E^+$, several orders of magnitude higher than those of **P10**. Extensional results for samples **P1**−**P3** at a short time follow the linear viscoelastic envelope, whereas, at a long time, there is a distinct increase in extensional viscosity (strain hardening). Even though H-bonding represents a weak noncovalent interaction, several studies have demonstrated that systems with reversible associations induce strong strain-hardening effects.[38,76,77] As presented previously,[76,77] the extensional behavior of associating polymers strongly depends on the Weissenberg number. Even for the lowest Hencky strain rates, the *Wi* is much greater than 0.5 due to the long terminal relaxation for all polymers with H-bonding interactions. A final note is referred to shapes of the curves of **P1** and **P2** samples compared to those of **P3**. While all show strong strain-hardening effects, the **P3** curves after the initial strong strain-hardening growth exhibit a milder growth, which might be due to yielding of the polymer owing to the high molecular weight of the chain segments trapped between two physical bonds, $M_x$ (more intra- vs intermolecular associations).

## CONCLUSIONS

Our studies provide insight into the synthesis and complete characterization of amine-containing polymers with tunable rheological properties. In summary, we have devised a new

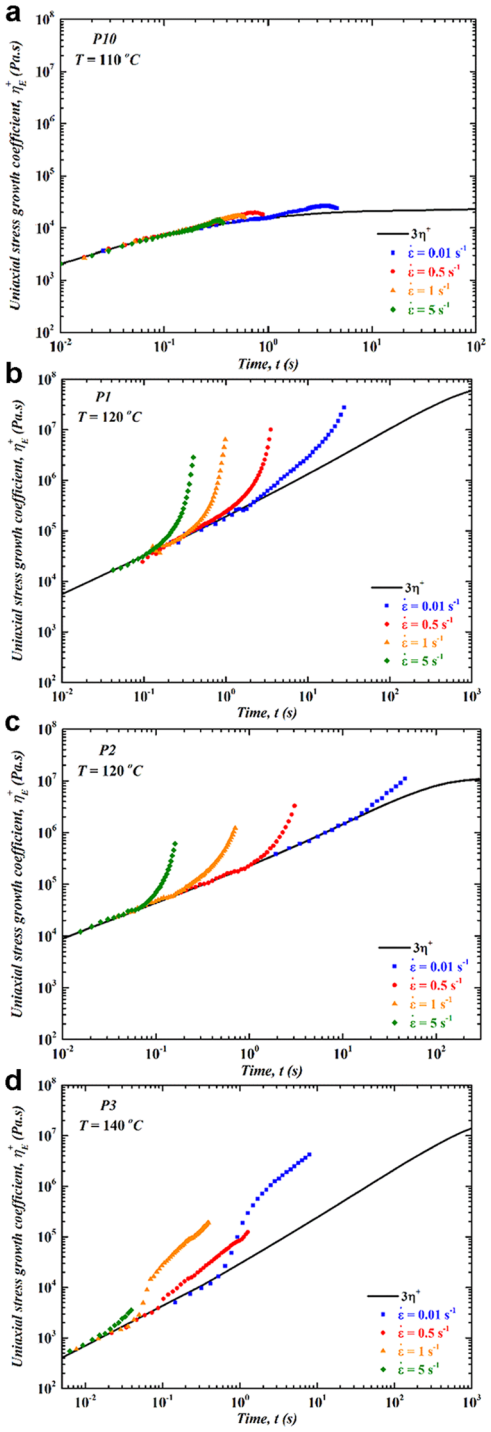


**Figure 5.** (a) Uniaxial stress growth coefficient obtained using a Sentmanat extensional rheometer at different Hencky strain rates from 0.01 to 5 $s^{-1}$ at the reference temperature of 110 °C of tertiary amine-containing polynorbornene, **P10** ($M_w$ = 175 700 g/mol). (b) Uniaxial stress growth coefficient obtained using a Sentmanat extensional rheometer at different Hencky strain rates from 0.01 to 5 $s^{-1}$ at the reference temperature of 120 °C of the **P1** sample ($M_w$ = 119 000 g/mol). (c) Uniaxial stress growth coefficient obtained using a Sentmanat extensional rheometer at different Hencky strain rates from 0.01 to 5 $s^{-1}$ at the reference temperature of 120 °C of the **P2** sample ($M_w$ = 113 600 g/mol). (d) Uniaxial stress growth coefficient obtained using a Sentmanat extensional rheometer at different Hencky strain rates from 0.01 to 5 $s^{-1}$ at the reference temperature of 140 °C of the **P3** sample ($M_w$ = 186 600 g/mol).


https://dx.doi.org/10.1021/acs.macromol.9b02158
Macromolecules 2020, 53, 2649−2661

catalytic protocol for monomer synthesis in one step from commercially available starting materials through the use of hydroaminoalkylation. Subsequent ROMP of these monomers results in polymers with controlled incorporation of a variety of H-bonding amine groups. The extensive thermorheological studies of the *sec*-amine-containing polymers showed solid-like behavior at time scales of about $10^8$ s and longer due to the extended H-bonding network among the polymer chains. The bulky side groups reduce the mobility and thus the number of physical entanglements becomes insignificant compared to the number of reversible associations. Therefore, their rheological behavior is entirely controlled by the dynamics of associations, offering an opportunity to study and test related theories of associating reversible polymeric networks. As a result of these reversible associations, strong strain-hardening effects are obtained. The long sticky-reptation times make $W_i$ extremely high even at the lowest Hencky strain rates. The H-bonding ability of the polymers can be tuned by exploiting different H-bond-accepting groups on the aryl ring and this, in turn, can tune the rheological properties of these polymers. On the contrary, the tertiary amine-containing polymers behave as liquid-like materials, indicating that the presence of the *sec*-amine hydrogen is essential for entanglement and cross-linking of the polymers. This strategy has opened a new avenue to make amine-functionalized materials with variable interesting bulk properties. Further studies involving polymers with alternative polyolefin backbones, different amine substituents, and variable amounts of amine incorporation are ongoing.

## EXPERIMENTAL SECTION

**General Details.** All of the experiments involving organometallic compounds were carried out in nitrogen-filled MBraun gloveboxes. All of the amine substrates for hydroaminoalkylation were purchased from Aldrich and purified by either sublimation or distillation over $CaH_2$ and degassed by three successive freeze−pump−thaw cycles before being placed inside the glovebox. Anhydrous solvents were obtained from an activated alumina tower and degassed prior to use. Toluene-$d_8$ was dried over activated 4 Å molecular sieves and degassed prior to use. High-resolution EI mass spectra (HRMS) were acquired from a Waters/Micromass LCT spectrometer. An Agilent 7890 A GC system was used for gas chromatography−mass spectrometry (GC−MS). Fourier transform infrared (FTIR) spectra were obtained from a PerkinElmer Frontier (attenuated total reflection (ATR)) spectrometer.

**NMR Spectroscopy.** NMR spectroscopy was performed on a Bruker Avance 300 or 400 MHz spectrometer at room temperature unless otherwise stated.

**Gel Permeation Chromatography.** All of the polymers were precipitated thrice in cold methanol, followed by in vacuo drying in a vacuum oven overnight prior to GPC runs. All of the GPC characterizations were done in high-performance liquid chromatography (HPLC)-grade THF at a flow rate of 1.0 mL/min using a Malvern OMNISEC GPC instrument equipped with a Viscotek TGuard guard column (CLM3008), and Viscotek T3000 (CLM3003) and T6000 (CLM3006) GPC columns packed with porous poly(styrene-*co*-divinylbenzene) particles regulated at room temperature. The instrument was equipped with triple detection to achieve the signal response from a differential viscometer, a differential refractive index (RI), and right- and low-angle light scattering detectors. Calibration of interdetector distances was performed using a polystyrene standard from Malvern Inc. The RI increments (d*n*/d*c*) were obtained using 100% mass recovery methods from Malvern OMNISEC software, with each polymer sample being run at least three times to ensure reproducibility.

**Differential Scanning Calorimetry.** The thermal properties of the samples were measured on a Netzsch DSC 214 Polyma differential scanning calorimeter. Analyses were performed in an inert atmosphere (nitrogen) with samples of approximately 5−10 mg in a ceramic pan. All analyses were conducted in duplicate. Samples were heated to 150 °C at a heating rate of 5 °C/min. They were held isothermally at 150 °C for 5 min to eliminate any thermal history, followed by gradual cooling to 0 °C at a cooling rate of 5 °C/min. The samples were then reheated to 150 °C at a heating rate of 5 °C/min. The glass transition temperatures were determined from the second heating ramp.

**Thermogravimetric Analysis.** A Netzsch TG 209 F1 Libra thermogravimetric analyzer was used for the thermogravimetrical experiments. All samples were primarily dried at 40 °C overnight. The tests of 4−10 mg of each sample were performed by continuously passing a high-purity nitrogen stream (99.5% $N_2$, 50 $cm^3$/min) into the furnace at a heating rate of 5 °C/min, from 25 to 600 °C.

**Linear Viscoelastic Measurements.** The Anton Paar MCR 702 device equipped with the cone-and-plate geometry (a standard 25 mm cone in diameter with an angle of 0.07 rad) was used to study the linear viscoelastic (LVE) properties of synthesized polymers. The thermal stability of samples was studied for 2 h isothermally at the reference temperature of 120 °C. The linear viscoelastic regime was identified by performing strain sweep experiments using strains from 0.001 to 1 at a constant frequency of 0.1 Hz. Frequency sweep experiments were performed within the linear viscoelastic region at various temperatures.

**Extensional Viscosity Measurements.** The second-generation Sentmanat extension rheometer (SER2) was used to measure the uniaxial stress growth coefficient as a function of time. Samples were cut into rectangular shapes (same size) and tested at various constant Hencky strain rates from 0.01 to 5 $s^{-1}$. Measurements were performed at the reference temperature of 120 °C, which was controlled with an air/nitrogen convection oven.

**General Procedure for Monomer Synthesis.** For the monomer synthesis, the required amounts of $Ta(NMe_2)_5$ and 3-methyl pyridone were weighed into a 20 mL scintillation vial inside a nitrogen-filled glovebox, followed by the addition of 2 mL of toluene. The required amounts of amine and norbornene were weighed in a separate scintillation vial and were subsequently added to the previous vial, followed by the addition of a magnetic stir bar. The vial was sealed with a Teflon cap and taken out of the glovebox, where it was heated at 130 °C in an oil bath for the required amount of time. Finally, the monomers were purified by column chromatography (SiliaFlash F-60, 230−400 mesh) using the solvent systems listed below.

**General Procedure for Polymer Synthesis.** The same method for polymerization was adopted as reported. A typical polymerization reaction is described for the polymerization of **M1** to generate **P1**. A solution of monomer (100 equiv, 0.200 g, 1.00 mmol) in 1 mL of dry, degassed THF was prepared under a nitrogen atmosphere. The solution was added to a vial containing a Grubbs second-generation catalyst (1 equiv, 8.5 mg, 0.01 mmol) and a magnetic stir bar. The mixture was stirred inside the nitrogen-filled glovebox at room temperature (25 °C) for 20 h and quenched by adding ethyl vinyl ether (excess, 5 equiv vs [Ru]). The reaction mixture usually turns deep brown or black over a 30 min duration. The reaction was added dropwise to a vortex of cold methanol (−35 °C), producing an off-white, flocculent solid. The precipitated polymer was collected by filtration and dried in vacuo overnight, and the percent yield was calculated gravimetrically (0.190 g, 95%). GPC characterization was performed on the material after the second precipitation to assure complete removal of the G2 from the polymer matrix. A minimum amount of 500 mg of polymer was required to carry out all of the rheological experiments. A similar procedure was adopted to make the polymer inside the glovebox, keeping the monomer concentration constant, i.e., 0.1 g/mL of solvent.

## ASSOCIATED CONTENT

### Supporting Information

The Supporting Information is available free of charge at https://pubs.acs.org/doi/10.1021/acs.macromol.9b02158.



https://dx.doi.org/10.1021/acs.macromol.9b02158
Macromolecules 2020, 53, 2649−2661

Experimental details; molecular characterization ($^{1}$H, $^{13}$C, and $^{19}$F NMR spectra); and polymer characterization (GPC traces, DSC, TGA, and rheological analyses) (PDF)

## AUTHOR INFORMATION


### Corresponding Authors

**Savvas G. Hatzikiriakos** − *Department of Chemical and Biological Engineering, University of British Columbia, Vancouver, British Columbia V6T 1Z3, Canada;* orcid.org/0000-0002-1456-7927; Email: savvas.hatzi@ubc.ca

**Laurel L. Schafer** − *Department of Chemistry, University of British Columbia, Vancouver, British Columbia V6T 1Z4, Canada;* orcid.org/0000-0003-0354-2377; Email: schafer@chem.ubc.ca

### Authors

**Nirmalendu Kuanr** − *Department of Chemistry, University of British Columbia, Vancouver, British Columbia V6T 1Z4, Canada*

**Tanja Tomkovic** − *Department of Chemical and Biological Engineering, University of British Columbia, Vancouver, British Columbia V6T 1Z3, Canada;* orcid.org/0000-0002-1144-2723

**Damon J. Gilmour** − *Department of Chemistry, University of British Columbia, Vancouver, British Columbia V6T 1Z4, Canada*

**Mitchell R. Perry** − *Department of Chemistry, University of British Columbia, Vancouver, British Columbia V6T 1Z4, Canada*

**Shou-Jen Hsiang** − *Department of Chemistry, University of British Columbia, Vancouver, British Columbia V6T 1Z4, Canada*

**Evelyne van Ruymbeke** − *Bio and Soft Division (BSMA), Institute of Condensed Matter and Nanosciences (IMCN), Universite catholique de Louvain, B-1348 Louvain-la-Neuve, Belgium;* orcid.org/0000-0001-7633-0194

Complete contact information is available at: https://pubs.acs.org/10.1021/acs.macromol.9b02158

### Author Contributions

$^{\parallel}$N.K. and T.T. have contributed equally to this work.


### Notes

The authors declare no competing financial interest.

## ACKNOWLEDGMENTS

The authors thank NSERC for financial support of this work. The authors also thank UBC for postgraduate scholarships. N.K. and D.J.G. also thank CREATE Sustainable Synthesis for funding. L.L.S. thanks the Canada Research Chairs program for supporting this work in part. The authors also thank Prof. Jason Hein and Thomas Malig for their assistance with the variable-temperature FTIR spectroscopy experiments. E.V.R. is Research Associate of FSR-FNRS and thanks DoDyNet (H2020 - MSCA- ITN 765811) for financial support.

## REFERENCES


(1) Long, B. K.; Eagan, J. M.; Mulzer, M.; Coates, G. W. Semi-Crystalline Polar Polyethylene: Ester-Functionalized Linear Polyolefins Enabled by a Functional-Group-Tolerant, Cationic Nickel Catalyst. *Angew. Chem., Int. Ed.* **2016**, *55*, 7106−7110.

(2) Jian, Z.; Mecking, S. Short-Chain Branched Polar-Functionalized Linear Polyethylene via "Tandem Catalysis". *Macromolecules* **2016**, *49*, 4057−4066.

(3) Godoy Lopez, R.; D'Agosto, F.; Boisson, C. Synthesis of well-defined polymer architectures by successive catalytic olefin polymerization and living/controlled polymerization reactions. *Prog. Polym. Sci.* **2007**, *32*, 419−454.

(4) Boaen, N. K.; Hillmyer, M. A. Post-polymerization functionalization of polyolefins. *Chem. Soc. Rev.* **2005**, *34*, 267−275.

(5) Blasco, E.; Sims, M. B.; Goldmann, A. S.; Sumerlin, B. S.; Barner-Kowollik, C. 50th Anniversary Perspective: Polymer Functionalization. *Macromolecules* **2017**, *50*, 5215−5252.

(6) Öztürk, B. Ö.; Yakut, E.; Ak, E.; Şehitoğlu, S. K. Imidazole-substituted ROMP polymers: Post-modification of poly(norbornenediester) derivatives with aminolysis reactions. *React. Funct. Polym.* **2017**, *111*, 22−29.

(7) Slugovc, C. The Ring Opening Metathesis Polymerisation Toolbox. *Macromol. Rapid Commun.* **2004**, *25*, 1283−1297.

(8) Leitgeb, A.; Wappel, J.; Slugovc, C. The ROMP toolbox upgraded. *Polymer* **2010**, *51*, 2927−2946.

(9) Perry, M. R.; Ebrahimi, T.; Morgan, E.; Edwards, P. M.; Hatzikiriakos, S. G.; Schafer, L. L. Catalytic Synthesis of Secondary Amine-Containing Polymers: Variable Hydrogen Bonding for Tunable Rheological Properties. *Macromolecules* **2016**, *49*, 4423−4430.

(10) Garcia, P.; Lau, Y. Y.; Perry, M. R.; Schafer, L. L. Phosphoramidate Tantalum Complexes for Room-Temperature C-H Functionalization: Hydroaminoalkylation Catalysis. *Angew. Chem., Int. Ed.* **2013**, *52*, 9144−9148.

(11) Chong, E.; Garcia, P.; Schafer, L. L. Hydroaminoalkylation: Early-Transition-Metal-Catalyzed $\alpha$-Alkylation of Amines. *Synthesis* **2014**, *46*, 2884−2896.

(12) Brandt, J. W.; Chong, E.; Schafer, L. L. Ligand Effects and Kinetic Investigations of Sterically Accessible 2-Pyridonate Tantalum Complexes for Hydroaminoalkylation. *ACS Catal.* **2017**, *7*, 6323−6330.

(13) Edwards, P. M.; Schafer, L. L. In Situ Generation of a Regio- and Diastereoselective Hydroaminoalkylation Catalyst Using Commercially Available Starting Materials. *Org. Lett.* **2017**, *19*, 5720−5723.

(14) Lauzon, J. M.; Eisenberger, P.; Roşca, S.-C.; Schafer, L. L. Amidate Complexes of Tantalum and Niobium for the Hydroaminoalkylation of Unactivated Alkenes. *ACS Catal.* **2017**, *7*, 5921−5931.

(15) DiPucchio, R. C.; Roşca, S.-C.; Schafer, L. L. Catalytic and Atom-Economic C−C Bond Formation: Alkyl Tantalum Ureates for Hydroaminoalkylation. *Angew. Chem.* **2018**, *130*, 3527−3530.

(16) Buchmeiser, M. R.; Sen, S.; Unold, J.; Frey, W. N-Heterocyclic Carbene, High Oxidation State Molybdenum Alkylidene Complexes: Functional-Group-Tolerant Cationic Metathesis Catalysts. *Angew. Chem., Int. Ed.* **2014**, *53*, 9384−9388.

(17) Alfred, S. F.; Lienkamp, K.; Madkour, A. E.; Tew, G. N. Water-soluble ROMP polymers from amine-functionalized norbornenes. *J. Polym. Sci., Part A: Polym. Chem.* **2008**, *46*, 6672−6676.

(18) Noro, A.; Matsushima, S.; He, X.; Hayashi, M.; Matsushita, Y. Thermoreversible supramolecular polymer gels via metal−Ligand coordination in an ionic liquid. *Macromolecules* **2013**, *46*, 8304−8310.

(19) Kumpfer, J. R.; Jin, J.; Rowan, S. J. Stimuli-responsive europium-containing metallo-supramolecular polymers. *J. Mater. Chem.* **2010**, *20*, 145−151.

(20) Burnworth, M.; Tang, L.; Kumpfer, J. R.; Duncan, A. J.; Beyer, F. L.; Fiore, G. L.; Rowan, S. J.; Weder, C. Optically healable supramolecular polymers. *Nature* **2011**, *472*, 334−337.

(21) Hayashi, M.; Noro, A.; Matsushita, Y. Viscoelastic properties of supramolecular soft materials with transient polymer network. *J. Polym. Sci., Part B: Polym. Phys.* **2014**, *52*, 755−764.

(22) Oku, T.; Furusho, Y.; Takata, T. A Concept for Recyclable Cross-Linked Polymers: Topologically Networked Polyrotaxane

Capable of Undergoing Reversible Assembly and Disassembly. *Angew. Chem., Int. Ed.* **2004**, *43*, 966−969.
(23) Ogawa, M.; Kawasaki, A.; Koyama, Y.; Takata, T. Synthesis and properties of a polyrotaxane network prepared from a Pd-templated bis-macrocycle as a topological cross-linker. *Polym. J.* **2011**, *43*, 909−915.
(24) Huh, K. M.; Cho, Y. W.; Chung, H.; Kwon, I. C.; Jeong, S. Y.; Ooya, T.; Lee, W. K.; Sasaki, S.; Yui, N. Supramolecular Hydrogel Formation Based on Inclusion Complexation Between Poly (ethylene glycol)-Modified Chitosan and α-Cyclodextrin. *Macromol. Biosci.* **2004**, *4*, 92−99.
(25) Yan, X.; Wang, F.; Zheng, B.; Huang, F. Stimuli-responsive supramolecular polymeric materials. *Chem. Soc. Rev.* **2012**, *41*, 6042−6065.
(26) Danila, I.; Riobe, F.; Piron, F.; Puigmartí-Luis, J.; Wallis, J. D.; Linares, M.; Ågren, H.; Beljonne, D.; Amabilino, D. B.; Avarvari, N. Hierarchical Chiral Expression from the Nano-to Mesoscale in Synthetic Supramolecular Helical Fibers of a Nonamphiphilic C 3-Symmetrical π-Functional Molecule. *J. Am. Chem. Soc.* **2011**, *133*, 8344−8353.
(27) Herbst, F.; Döhler, D.; Michael, P.; Binder, W. H. Self-Healing Polymers via Supramolecular Forces. *Macromol. Rapid Commun.* **2013**, *34*, 203−220.
(28) Ge, Z.; Hu, J.; Huang, F.; Liu, S. Responsive supramolecular gels constructed by crown ether based molecular recognition. *Angew. Chem., Int. Ed.* **2009**, *48*, 1798−1802.
(29) Yan, X.; Xu, D.; Chi, X.; Chen, J.; Dong, S.; Ding, X.; Yu, Y.; Huang, F. A multiresponsive, shape-persistent, and elastic supramolecular polymer network gel constructed by orthogonal self-assembly. *Adv. Mater.* **2012**, *24*, 362−369.
(30) Weng, W.; Beck, J. B.; Jamieson, A. M.; Rowan, S. J. Understanding the mechanism of gelation and stimuli-responsive nature of a class of metallo-supramolecular gels. *J. Am. Chem. Soc.* **2006**, *128*, 11663−11672.
(31) Wojtecki, R. J.; Meador, M. A.; Rowan, S. J. Using the dynamic bond to access macroscopically responsive structurally dynamic polymers. *Nat. Mater.* **2011**, *10*, 14−27.
(32) Brunsveld, L.; Folmer, B.; Meijer, E. W.; Sijbesma, R. Supramolecular polymers. *Chem. Rev.* **2001**, *101*, 4071−4098.
(33) de Espinosa, L. M.; Fiore, G. L.; Weder, C.; Foster, E. J.; Simon, Y. C. Healable supramolecular polymer solids. *Prog. Polym. Sci.* **2015**, *49*−*50*, 60−78.
(34) Cordier, P.; Tournilhac, F.; Soulié-Ziakovic, C.; Leibler, L. Self-healing and thermoreversible rubber from supramolecular assembly. *Nature* **2008**, *451*, 977−980.
(35) Chen, Y.; Kushner, A. M.; Williams, G. A.; Guan, Z. Multiphase design of autonomic self-healing thermoplastic elastomers. *Nat. Chem.* **2012**, *4*, 467−472.
(36) Courtois, J.; Baroudi, I.; Nouvel, N.; Degrandi, E.; Pensec, S.; Ducouret, G.; Chanéac, C.; Bouteiller, L.; Creton, C. Supramolecular Soft Adhesive Materials. *Adv. Funct. Mater.* **2010**, *20*, 1803−1811.
(37) Kautz, H.; Van Beek, D.; Sijbesma, R. P.; Meijer, E. Cooperative end-to-end and lateral hydrogen-bonding motifs in supramolecular thermoplastic elastomers. *Macromolecules* **2006**, *39*, 4265−4267.
(38) Shabbir, A.; Goldansaz, H.; Hassager, O.; Van Ruymbeke, E.; Alvarez, N. J. Effect of hydrogen bonding on linear and nonlinear rheology of entangled polymer melts. *Macromolecules* **2015**, *48*, 5988−5996.
(39) Cheng, C.-C.; Wang, J.-H.; Chuang, W.-T.; Liao, Z.-S.; Huang, J.-J.; Huang, S.-Y.; Fan, W.-L.; Lee, D.-J. Dynamic supramolecular self-assembly: hydrogen bonding-induced contraction and extension of functional polymers. *Polym. Chem.* **2017**, *8*, 3294−3299.
(40) Chen, S.; Binder, W. H. Dynamic ordering and phase segregation in hydrogen-bonded polymers. *Acc. Chem. Res.* **2016**, *49*, 1409−1420.
(41) Yount, W. C.; Juwarker, H.; Craig, S. L. Orthogonal control of dissociation dynamics relative to thermodynamics in a main-chain reversible polymer. *J. Am. Chem. Soc.* **2003**, *125*, 15302−15303.
(42) Serpe, M. J.; Craig, S. L. Physical organic chemistry of supramolecular polymers. *Langmuir* **2007**, *23*, 1626−1634.
(43) Xu, D.; Craig, S. L. Scaling laws in supramolecular polymer networks. *Macromolecules* **2011**, *44*, 5465−5472.
(44) Hourdet, D.; Gadgil, J.; Podhajecka, K.; Badiger, M. V.; Brûlet, A.; Wadgaonkar, P. P. Thermoreversible behavior of associating polymer solutions: thermothinning versus thermothickening. *Macromolecules* **2005**, *38*, 8512−8521.
(45) Nair, K. P.; Breedveld, V.; Weck, M. Complementary hydrogen-bonded thermoreversible polymer networks with tunable properties. *Macromolecules* **2008**, *41*, 3429−3438.
(46) David, R. L. A.; Wei, M.-H.; Liu, D.; Bathel, B. F.; Plog, J. P.; Ratner, A.; Kornfield, J. A. Effects of pairwise, self-associating functional side groups on polymer solubility, solution viscosity, and mist control. *Macromolecules* **2009**, *42*, 1380−1391.
(47) Nair, K. P.; Breedveld, V.; Weck, M. Modulating mechanical properties of self-assembled polymer networks by multi-functional complementary hydrogen bonding. *Soft Matter* **2011**, *7*, 553−559.
(48) Van Ruymbeke, E. Preface: Special issue on associating polymers. *J. Rheol.* **2017**, *61*, 1099−1102.
(49) Cates, M. Reptation of living polymers: dynamics of entangled polymers in the presence of reversible chain-scission reactions. *Macromolecules* **1987**, *20*, 2289−2296.
(50) Leibler, L.; Rubinstein, M.; Colby, R. H. Dynamics of reversible networks. *Macromolecules* **1991**, *24*, 4701−4707.
(51) Van Ruymbeke, E.; Keunings, R.; Bailly, C. Prediction of linear viscoelastic properties for polydisperse mixtures of entangled star and linear polymers: Modified tube-based model and comparison with experimental results. *J. Non-Newtonian Fluid Mech.* **2005**, *128*, 7−22.
(52) Schleyer, P. v. R.; Williams, J. E., Jr.; Blanchard, K. Evaluation of strain in hydrocarbons. The strain in adamantane and its origin. *J. Am. Chem. Soc.* **1970**, *92*, 2377−2386.
(53) Lummiss, J. A. M.; Ireland, B. J.; Sommers, J. M.; Fogg, D. E. Amine-Mediated Degradation in Olefin Metathesis Reactions that Employ the Second-Generation Grubbs Catalyst. *ChemCatChem* **2014**, *6*, 459−463.
(54) Lummiss, J. A. M.; McClennan, W. L.; McDonald, R.; Fogg, D. E. Donor-Induced Decomposition of the Grubbs Catalysts: An Intercepted Intermediate. *Organometallics* **2014**, *33*, 6738−6741.
(55) Walker, R.; Conrad, R. M.; Grubbs, R. H. The Living ROMP of trans-Cyclooctene. *Macromolecules* **2009**, *42*, 599−605.
(56) Nyström, A.; Malkoch, M.; Furó, I.; Nyström, D.; Unal, K.; Antoni, P.; Vamvounis, G.; Hawker, C.; Wooley, K.; Malmström, E.; Hult, A. Characterization of poly (norbornene) dendronized polymers prepared by ring-opening metathesis polymerization of dendron bearing monomers. *Macromolecules* **2006**, *39*, 7241−7249.
(57) Love, J. A.; Sanford, M. S.; Day, M. W.; Grubbs, R. H. Synthesis, structure, and activity of enhanced initiators for olefin metathesis. *J. Am. Chem. Soc.* **2003**, *125*, 10103−10109.
(58) Bielawski, C. W.; Grubbs, R. H. Increasing the initiation efficiency of ruthenium-based ring-opening metathesis initiators: effect of excess phosphine. *Macromolecules* **2001**, *34*, 8838−8840.
(59) Esteruelas, M. A.; González, F.; Herrero, J.; Lucio, P.; Oliván, M.; Ruiz-Labrador, B. Thermal properties of polynorbornene (cis-and trans-) and hydrogenated polynorbornene. *Polym. Bull.* **2007**, *58*, 923−931.
(60) Cataldo, F. FTIR spectroscopic characterization of hydrogenated polyoctenamer and polynorbornene and DSC study of their thermal properties. *Polym. Int.* **1994**, *34*, 49−57.
(61) Dealy, J. M.; Read, D. J.; Larson, R. G. *Structure and Rheology of Molten Polymers: From Structure to Flow Behavior and Back Again*, 2nd ed.; Carl Hanser Verlag GmbH Co KG, 2018.
(62) Rubinstein, M.; Colby, R. H. *Polymer Physics*; Oxford University Press: New York, 2003; Vol. 23.
(63) Zhang, Z.; Chen, Q.; Colby, R. H. Dynamics of associative polymers. *Soft Matter* **2018**, *14*, 2961−2977.
(64) Chen, Q.; Zhang, Z.; Colby, R. H. Viscoelasticity of entangled random polystyrene ionomers. *J. Rheol.* **2016**, *60*, 1031−1040.


https://dx.doi.org/10.1021/acs.macromol.9b02158
*Macromolecules* 2020, 53, 2649−2661

(65) Hawke, L.; Ahmadi, M.; Goldansaz, H.; Van Ruymbeke, E. Viscoelastic properties of linear associating poly (n-butyl acrylate) chains. *J. Rheol.* **2016**, *60*, 297−310.
(66) Rubinstein, M.; Semenov, A. N. Dynamics of entangled solutions of associating polymers. *Macromolecules* **2001**, *34*, 1058−1068.
(67) Cates, M. E.; McLeish, T. C. B.; Rubinstein, M. 'Living trees': dynamics at a reversible classical gel point. *J. Phys.: Condens. Matter* **1990**, *2*, 749−754.
(68) Yount, W. C.; Loveless, D. M.; Craig, S. L. Small-molecule dynamics and mechanisms underlying the macroscopic mechanical properties of coordinatively cross-linked polymer networks. *J. Am. Chem. Soc.* **2005**, *127*, 14488−14496.
(69) Sprakel, J.; van der Gucht, J.; Stuart, M. A. C.; Besseling, N. A. Brownian particles in transient polymer networks. *Phys. Rev. E* **2008**, *77*, No. 061502.
(70) Rubinstein, M.; Semenov, A. N. Thermoreversible gelation in solutions of associating polymers. 2. Linear dynamics. *Macromolecules* **1998**, *31*, 1386−1397.
(71) Doi, M.; Edwards, S. F. *The Theory of Polymer Dynamics*; Clarendon Press: Oxford, 1988.
(72) de Gennes, P.-G. Reptation of a polymer chain in the presence of fixed obstacles. *J. Chem. Phys.* **1971**, *55*, 572−579.
(73) Van Ruymbeke, E.; Orfanou, K.; Kapnistos, M.; Iatrou, H.; Pitsikalis, M.; Hadjichristidis, N.; Lohse, D.; Vlassopoulos, D. Entangled dendritic polymers and beyond: Rheology of symmetric Cayley-tree polymers and macromolecular self-assemblies. *Macromolecules* **2007**, *40*, 5941−5952.
(74) Van Ruymbeke, E.; Bailly, C.; Keunings, R.; Vlassopoulos, D. A general methodology to predict the linear rheology of branched polymers. *Macromolecules* **2006**, *39*, 6248−6259.
(75) Fox, J. D.; Rowan, S. J. Supramolecular polymerizations and main-chain supramolecular polymers. *Macromolecules* **2009**, *42*, 6823−6835.
(76) Arora, S.; Shabbir, A.; Hassager, O.; Ligoure, C.; Ramos, L. Brittle fracture of polymer transient networks. *J. Rheol.* **2017**, *61*, 1267−1275.
(77) Shabbir, A.; Huang, Q.; Baeza, G. P.; Vlassopoulos, D.; Chen, Q.; Colby, R. H.; Alvarez, N. J.; Hassager, O. Nonlinear shear and uniaxial extensional rheology of polyether-ester-sulfonate copolymer ionomer melts. *J. Rheol.* **2017**, *61*, 1279−1289.


https://dx.doi.org/10.1021/acs.macromol.9b02158
*Macromolecules* 2020, 53, 2649−2661